



Preparation of Pd-Coated Anodic Alumina Membranes for Gas Separation Media

Rosalinda Inguanta, Mariateresa Amodeo, Fabio D'Agostino, Maurizio Volpe, Salvatore Piazza, and Carmelo Sunseri^{*z}

Dipartimento di Ingegneria Chimica dei Processi e dei Materiali, Università di Palermo, 90128 Palermo, Italy

Different procedures of Pd electroless deposition onto anodic alumina membranes were investigated to form a dense metal layer covering pores. The main difficulty was related to the amorphous nature of anodic alumina membranes, determining low chemical stability in solutions at pH > 9, where Pd plating works more efficiently. As a consequence, it was necessary to find the operative conditions allowing Pd deposition without damaging the membrane: to reduce alumina dissolution, the plating bath was buffered at pH 8.5 by addition of either NaHCO₃ or Na₂B₄O₇·H₂O. Acceptable conversion of Pd was found after a deposition time of 3 min. Single and multiple deposition steps (each lasting 3 min) were accomplished. After five deposition steps, pores remained open in the plating bath containing NaHCO₃, while they were almost totally occluded in the bath containing Na₂B₄O₇·H₂O. In this last bath, a dense layer of Pd, ~1 μm thick, was obtained after four deposition steps alternated with surface reactivation steps; the complete closure of pores was confirmed by gas permeability measurements. The different behavior of the two buffers can be attributed to a higher solubility of amorphous alumina in NaHCO₃ solution.

© 2007 The Electrochemical Society. [DOI: 10.1149/1.2432067] All rights reserved.

Manuscript submitted September 11, 2006; revised manuscript received November 8, 2006.
Available electronically February 2, 2007.

Porous alumina layers can be formed by anodic oxidation of aluminium in suitable electrolytes, where the oxide is sparingly soluble. Typically, aqueous solutions of inorganic and organic acid, like sulfuric, phosphoric, chromic, and oxalic acid, were used to grow anodic porous layers with morphology dependent on the anodizing conditions. Recently, anodizing of aluminium in aqueous solutions of organic acid electrolytes,¹⁻³ and in mixed solutions of sulfuric acid with addition of salicylic acid was also proposed. In this last case, the use of salicylic acid allows the control of the optical properties of anodic alumina membranes (AAMs).⁴

The characteristic feature of porous layers obtained by aluminium anodizing is the high order degree of the porous structure, characterized by a close-packed array of columnar hexagonal cells, each containing a central pore normal to the oxide layer surface.⁵ It was assumed that parallelism of pore channels is due to the equilibrium between two processes: the field-enhanced oxide dissolution at the oxide/electrolyte interface, and the oxide growth at the metal/oxide interface.⁶⁻⁸ The growth of porous structures by aluminium anodizing was extensively investigated in the past, particularly to fabricate protective, corrosion-resistant coatings.⁹

The highly ordered porous structure makes anodic alumina an ideal host or template for the fabrication of nanostructured materials for applications in optoelectronics, sensors, magnetics, and electronic circuits.¹⁰⁻¹⁹

The recent ascendant interest in the fabrication of such porous structures is also due to the possibility of obtaining membranes, after removal of the residual metal and dissolution of the barrier layer separating the porous oxide from the anodizing aluminium.²⁰⁻²⁷ These membranes are of great interest in separation processes, such as micro- and ultrafiltration under severe conditions where organic membranes cannot be used, as well as for fabrication of catalytic membrane reactors (CMR), which exhibit higher conversion, selectivity, and yield compared with conventional reactors. Hydrogenation and dehydrogenation reactions are the most promising to be carried out in a CMR.^{28,29} Recently, attention was focused on reforming reactions of light hydrocarbons and/or methanol to produce hydrogen for energetics.^{30,31} In addition, pure hydrogen production for metallurgical applications and semiconductor fabrication are interesting. CMRs involving hydrogen, either as reagent or product, use palladium metal as permselective element. Because palladium is very expensive, employment of self-standing mem-

branes would be highly disadvantageous, so that composite membranes, consisting of a thin film of palladium deposited onto a porous support, are preferred. Different types of composite membranes were proposed depending on the support and on the preparation method of the palladium layer. For operations either at high temperature or in aggressive environment, inorganic support, such as porous stainless steel³² or γ-alumina³³ are used. The thin film of palladium can be deposited by different procedures, like chemical vapor deposition (CVD),³⁴ electroless plating,³² and electro-deposition.³⁵ In particular, electroless deposition is an easy and fast method to carry out compared to other ones.

In this work, we present a modified process of electroless deposition of palladium onto AAM prepared in phosphoric acid solution. AAMs are a suitable support for a palladium thin film because they are easy to prepare and exhibits low resistance to mass transport due to their ordered structure; unfortunately, they are not stable both in acidic and in alkaline solutions owing to their amorphous nature. The low chemical stability represents a severe limitation for Pd electroless deposition, because the possible baths have pH external to the stability interval of AAM. In fact, the optimum pH for palladium deposition was reported to be about 10,³⁶ but at this pH the membrane is chemically unstable. For these reasons, a systematic study was undertaken to detect conditions optimizing characteristics of palladium deposit and membrane stability. In a previous work,³⁷ we proposed a procedure giving a deposit of palladium after 30 min of immersion of the membrane in a bath having pH 8.4. However, with this procedure Pd deposition was localized at the pore mouth, so that the channels were not occluded and the composite membranes are suitable only for catalysis, but not for gas separation. Another limit of this procedure was the slight damage and the enhanced fragility of membranes after 30 min deposition. Based on preliminary investigations showing that the conversion of palladium occurs predominantly in the first minutes, a novel procedure based on a shorter time of deposition and on the use of an appropriate pH stabilizer was developed. According to this procedure, complete occlusion of membrane channels was achieved, as shown by scanning electron microscopy and permeability measurements.

Experimental

Preparation of porous support.—The aluminium specimens, used to grow anodic porous layers, were 100 μm thick foils, 99.99% purity. High purity metal was preferred to minimize breakdown phenomena and the formation of flaws or cracks in the porous matrix. Prior to anodizing, samples were degreased with acetone and then they were electropolished at 20 V for 5 min in a HClO₄:C₂H₅OH

* Electrochemical Society Active Member.

^z E-mail: sunseri@dicpm.unipa.it

Table I. Composition of the sensitizing, activation and plating baths for electroless deposition of Pd.

Sensitizing solution (1 L)		Activation solution (1 L)	
SnCl ₂ ·2H ₂ O	1 g	Pd(NH ₃) ₄ (NO ₃) ₂ (10% solution)	1.5 mL
HCl (37%)	1 mL	HCl (37%)	1 mL
Palladium plating bath composition (1 L)			
Palladium precursor	Pb(NH ₃) ₄ (NO ₃) ₂ (10% solution)		25 mL
Complexing agent	Na ₂ EDTA		70 g
Buffer	NH ₃ ·H ₂ O (25%)		20 mL
	NaHCO ₃		2.6 g
	or		
	NH ₃ ·H ₂ O (25%)		20 mL
	0.025 M borax, 1 M HCl		25 mL
Reducing agent	N ₂ H ₄ (1 M)		17.8 mL

solution (1:6 by volume) vigorously stirred. Electrodes were mounted onto a holder to have a flat circular surface (39 mm diam) exposed to the solution, whose temperature was fixed at $-1 \pm 1^\circ\text{C}$ by means of a Lauda refrigerator (model RE 106). Electrolyte temperature was chosen to attain "hard anodizing" conditions, where a hard and abrasion resistant anodic layer is formed.⁹ Anodizing was conducted in 0.4 M H₃PO₄ solution in two steps: in the first, cell voltage was raised using a linear potential scan at 0.2 V s⁻¹ up to 160 V, while in the second one, the final voltage was held constant allowing to pass a potentiostatic charge of 160 C cm⁻². A Glassman High Tension power source (series ER) was used. The detachment of anodic oxide layer from the remaining metal was performed by chemical dissolution in a 0.1 M CuCl + 20% w/w HCl solution at 5°C. Pore bottom opening was achieved by immersion in 1 M NaOH solution at room temperature for 20 min. This treatment was made only on the metal-side surface to avoid enlargement of pore on the solution-side surface.

The morphological features of membranes were determined by SEM analysis (Philips model X30 ESEM).

Deposition of palladium.—To achieve a good metal film adhesion and to control electroless plating, surface cleaning and activation were essential. Surface cleaning was performed by a four-step procedure. AAMs were sonicated for 1 min at room temperature in an alkaline aqueous solution (1 g/L NaOH), then they were sonicated for 2 min in distilled water. After the ultrasonic treatment, membranes were rinsed with isopropyl alcohol for 10 min and with distilled water for a further 10 min. The cleaned membrane was dried in oven at 333 K for at least 4 h. After the cleaning procedure, the porous support surface was seeded with Pd nuclei, which initiates the autocatalytic reduction of the palladium complex in the subsequent plating step. Several methods for surface activation are reported in the literature.^{38,39} All of these methods are based on the use of solutions containing Sn²⁺ ions, therefore lowering the purity of the palladium layer. In this work, the two-step immersion procedure was preferred because the amount of tin in the final deposit was less.⁴⁰ This procedure consists in an alternate sequence of sensitizing steps, performed by immersion in SnCl₂/HCl aqueous solution, followed by dipping in the activation bath, this last being an acidic aqueous solution containing a Pd salt. Compositions of sensitizing and activation baths are reported in Table I.

A fresh stannous chloride solution was used after five sensitizing steps, because coalescence and precipitation of the suspended colloidal particles of SnCl₂ occurred after a few hours. On the contrary, the palladium solution was left to stabilize overnight before using and it could be stored for several days. A typical sensitizing-activation cycle was 2 min in sensitizing solution, 30 s in distilled water, 2 min in activation solution, and 30 s in distilled water.

The procedure was conducted at room temperature and it was

repeated ten times to obtain an optimal activated surface. The activated membrane was left drying in oven at 333 K overnight prior to palladium deposition.

Sn Mössbauer spectroscopy was carried to study the membrane surface after activation. Mössbauer spectra were recorded with a conventional spectrometer (RITVERC GmbH) operating in the transmission mode and having a Ca¹¹⁹SnO₃ source. Calibration was performed with spectra from Ca¹¹⁹SnO₃ and ⁵⁷Fe. The absorber samples were placed on the sample holder of a liquid N₂ cryostat (A.E.R.E. Harwell).

Palladium catalytic deposition was performed in a cylindrical Pyrex flask filled with 10 mL of plating solution. The deposition temperature was controlled at 333 K ± 1 K. After preheating the solution for 5 min, the reducing agent was added to the system and the solution was vigorously stirred before introducing the membrane.

The composition of the plating bath, reported in Table I, was specifically formulated to obtain a pH equal to 8.5. The amount of ammonia necessary to stabilize palladium species in solution was determined by a standard acid-base titration. The solution was buffered by a suitable quantity of either sodium hydrogen carbonate or borax to avoid dangerous changes of pH during plating. Hydrazine was used as reducing agent rather than hypophosphite, because oxidation of the latter produces hydrogen gas that could lead to a lower quality of palladium deposit.⁴¹ For each deposition, the efficiency of conversion was evaluated as ratio of the mass (mol) of palladium deposited to the mass of palladium in the bath.

The metal coating was characterized by scanning electron microscopy (SEM), X-ray diffraction (XRD), and energy dispersive spectroscopy (EDS). XRD patterns were obtained using a Philips generator (model PW 1130) and a PW goniometry (model 1050). The copper K α radiation and a scanning rate of 2 degree min⁻¹ were used. Measured d-spacings were compared with the ASTM index values. The distribution of Pd on the AAM surfaces and inside the channels was determined by a Philips EDX microprobe (model PV7760). The amount of palladium deposited was determined by atomic absorption spectroscopy (AAS), using a Varian spectrophotometer (model 100 Plus). Before AAS, the composite membrane was immersed in 5 mL of 1 M NaOH solution, where it was fully dissolved. The palladium particles were oxidized to Pd²⁺ by addition of 2 mL of 37% (w/w) HCl and 2 mL of 65% (w/w) HNO₃. This solution was diluted by addition of distilled water in order to reach a palladium concentration detectable by AAS. To avoid depressing of the atomic absorption signal due to aluminium ions, EDTA was added to all samples prior to analyzing.

Permeabilities of gases (H₂, He, CH₄, and N₂), through both the as-grown AAM and composite Al₂O₃-Pd membrane, were measured with a homemade permeation cell at room temperature. The gas flow rate was measured with a soap-bubble flow-meter at different trans-membrane pressures while the permeated side was kept at atmospheric pressure.

Results and Discussion

Cleaning and sensitizing/activation.—After anodizing, membranes exhibited the morphological features shown by the SEM pictures of Fig. 1, where Fig. 1a and b are relative to the solution-side surface and to the metal-side surface, respectively. This figure shows an asymmetrical pore structure on the two surfaces, with higher interpore wall thickness for the membrane surface formed in contact with the electrolyte. The different morphology can be attributed to the fabrication procedure of AAM: the formation of fresh oxide occurs only at the metal/oxide interface, owing to the reaction of Al³⁺ ions formed with O²⁻ ions migrating from the oxide/electrolyte interface, where they are injected into the oxide simultaneously with the ejection in solution of Al³⁺.^{7,8} As a consequence, pores on the solution-side surface are due to the anodizing process and they are formed in the initial stages of anodizing, while pores on the internal surface are formed by chemical dissolution of the barrier oxide layer

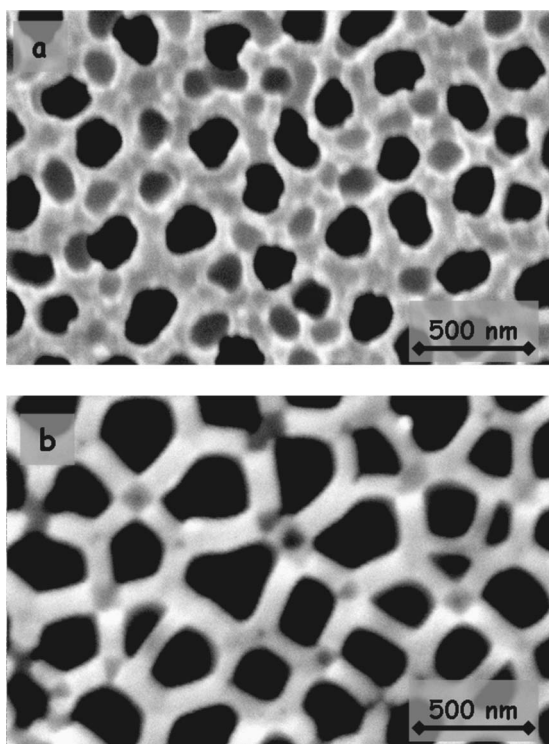


Figure 1. SEM images of anodic alumina membranes prepared in 0.4 M H_3PO_4 at 160 V – 1 °C and 160 C cm^{-2} : (a) solution side; and (b) metal side after dissolution of barrier layer in 1 M NaOH solution.

and they are formed after the anodizing process. Of course, the average pore size on this last surface depends on the dissolution conditions: for example, the morphology of Fig. 1b was obtained after chemical etching of the metal-side surface in 1 M NaOH at room temperature for 20 min. Prior to electroless deposition, membrane was cleaned in 1 g L^{-1} NaOH aqueous solution, which is aggressive toward amorphous alumina. As a consequence, an enlargement of about 20% of pore size and a thickness reduction (from 60 to about 54 μm) were observed.

The successive sensitizing/activation treatment plays a fundamental role in the electroless deposition of a metal on a nonconductive surface, because it leads to the formation of catalytic seeds. In this case, clusters of Sn-Pd, uniformly distributed onto the surface were formed. In particular, during the sensitizing step, a colloidal form of Sn^{2+} is deposited,^{39,40} while during the successive activation step the Pd^{2+} species is reduced to Pd^0 according to the reaction



The complete oxidation of Sn^{2+} to Sn^{4+} was confirmed by the Mössbauer analysis (Fig. 2), showing the presence of only Sn^{4+} on the membrane surface soon after the sensitizing/activation treatment. In fact, Fig. 2 shows only a large band at an isomer shift of 0 mm s^{-1} , typical of Sn^{4+} , while the doublet typical of Sn^{2+} at isomer shift of 2.55 mm s^{-1} is absent.⁴²

Atomic absorption analysis revealed that the total amount of Pd deposited during the activation step was about 2.93×10^{-2} mg cm^{-2} , while EDS analysis revealed different concentrations of Pd and Sn on the two surfaces, as shown in Table II. This difference can be attributed to the different morphology of the two surfaces, and in particular to the different membrane specific surface (ratio of the Al_2O_3 mass to the apparent surface) exposed to the sensitizing/activation solution. This interpretation is supported by data in Table II, showing that the highest amount of Sn and Pd was deposited on the solution-side surface, which exhibits a higher specific surface. However, from Table II a nearly equal Pd/Sn ratio in the catalytic particles is derived for both surfaces.

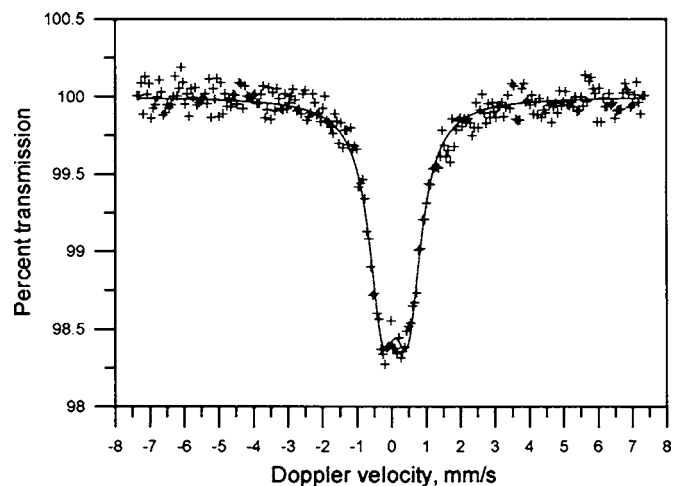


Figure 2. Mössbauer spectrum of an activated membrane showing the presence of tetraivalent tin sites only.

Electroless deposition.— Different parameters, like pH, time, and number of deposition steps were investigated to evaluate their influence on the final characteristics of the deposited film. pH was fixed at the value of either 10.0 or 8.5. In the last case, two different buffers, $\text{NaHCO}_3/\text{NH}_3$ and $\text{Na}_2\text{B}_4\text{O}_7 \cdot \text{H}_2\text{O}/\text{HCl}$, were used. Because pH plays a fundamental role on the electroless deposition process, in the following we present separately the results obtained according to both pH values.

$\text{NaHCO}_3/\text{NH}_3$, pH 10.— Initially, deposition was carried out at pH 10 to increase the conversion of palladium. From a thermodynamic point of view, an increase of pH favors the conversion, because hydrazine is a better reducing agent in an alkaline rather than in acidic medium. In fact, redox potentials are⁴³



in basic or acidic solution, respectively.

pH also affects the chelating action of EDTA and thus the conversion of palladium. At low pH, the degree of ionization of EDTA is low; therefore the concentration of free palladium ions in the solution is high because the chelating action is weak. As a result, the deposition bath is unstable, because the reduction of palladium ions can occur not only on the membrane surface but also on Pd nuclei formed in the bulk of solution. The solution turns to black and no Pd ions are available for plating. On the contrary, as pH increases, the chelating action of EDTA is enhanced because it is highly dissociated. As a result, the concentration of free palladium ions in solution is low, and the reduction is confined to the catalytic seeds on the membrane surface. At very high pH the fully ionized chelate anion forms the strongest metal chelate (Pd-EDTA) complex. In this case, the deposition of Pd is hindered because the concentration of Pd ions in solution is very low. Thus pH values between 9 and 11 enhance Pd conversion for the combined effect of both the redox potential of the reducing agent and the chelating action of EDTA.³⁶

The X-ray pattern of Fig. 3, relative to a membrane held for 3 min in the deposition bath at pH 10, shows the presence of palladium onto the membrane surface, while the broad band at about

Table II. Surface atomic ratio of anodic alumina membranes after sensitizing-activation treatment.

	Solution side	Metal side
Sn/Al atom %	0.264	0.094
Pd/Al atom %	0.091	0.033

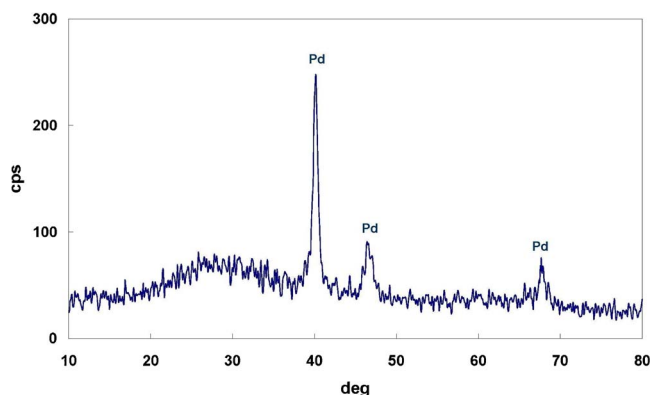


Figure 3. (Color online) XRD pattern of Pd-Al₂O₃ composite membranes obtained after 3 min in a deposition bath buffered at pH 10 in the presence of NaHCO₃.

$2\theta=28^\circ$ reveals the amorphous nature of the AAM. By using the Scherrer formula,⁴⁴ we calculated a grain size of about 11.5 nm. AAS revealed that the total amount of palladium deposited in these conditions was 0.205 mg cm⁻². The conversion was 53%, and the rate of deposition was 2.7×10^{-2} mg s⁻¹.

EDS analysis revealed surface concentrations of Pd on the two surfaces of about 53 and 47 atom %. This difference can be attributed to the different surface concentrations of catalytic sites formed during the sensitizing/activation treatment (see Table II), considering that the highest Pd concentration was detected on the surface having a higher concentration of catalytic seeds. The SEM pictures reported in Fig. 4 show metal deposits consisting of spherical particles, about 40 nm large, deposited around pore mouth and white particles of different size distributed onto the surface. The single grain size of 11.5 nm was not detected because SEM resolution is

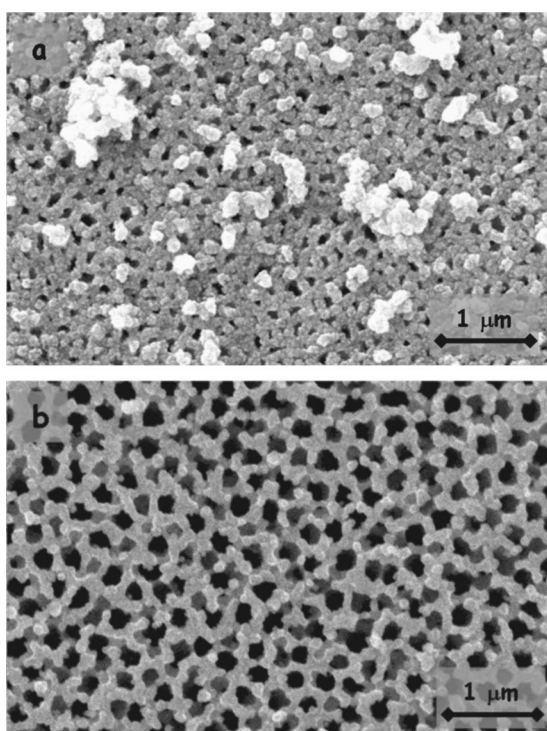


Figure 4. SEM micrographs of Pd-Al₂O₃ composite membranes obtained after 3 min in a deposition bath buffered at pH 10 in the presence of NaHCO₃: (a) solution side; and (b) metal side.

usually lower. Interestingly, Fig. 4 evidences that membrane surface was damaged with pore walls collapsed in many points (see Fig. 4b). Dissolution of AAM, at this pH, was confirmed by EDS analysis revealing that white particles consist of Pd, Al, and O, and by weight measurements, carried out before and after deposition, revealing a weight loss of about 9% for the membrane. Considering the weight gain due to metal deposition, the true weight loss of alumina during the immersion in the deposition bath was still higher after only 3 min of immersion. The formation of the white clusters could originate from the precipitation of alumina from the solution caused by a local pH decrease associated with the oxidation of hydrazine (Reaction 2). The white clusters are not evident on the metal-side surface (Fig. 4b) because, during the electroless deposition, AAM was immersed horizontally into the solution with this surface toward the bottom of the cell. In conclusion, these deposition conditions caused membrane partial dissolution, enhancing its fragility, while pores remained almost completely open.

NaHCO₃ buffer, pH 8.5.— On the basis of previous result, deposition of palladium was investigated in a solution buffered at pH 8.5 by addition of NaHCO₃. Membranes were held for 3 min in this solution. At this pH, dissolution of alumina will be very slow, even if a reduction in the conversion of palladium is expected. The morphology of a membrane prepared in these conditions is similar to that of Fig. 4: pores were still open, but their size was reduced. Membrane was also slightly damaged in these conditions, as confirmed by the presence of the white clusters. To explain the dissolution process of alumina at this pH, we have to focus our attention on the electroless deposition reaction



Reaction 4 causes a local increase of pH, which could determine the dissolution of alumina, while the oxidation of hydrazine, causes a local decrease of pH. Because the cathodic area, where palladium is reduced, and anodic area, where hydrazine is oxidized, are in contact, it is highly probable that alumina in contact with higher pH locally dissolves and it precipitates from the solution zones at lower pH, forming clusters embedded of palladium. XRD analysis revealed the presence of Pd on both membrane surfaces, while AAS revealed a total amount of deposited metal of 0.104 mg cm⁻². Conversion and deposition rate of Pd were 27% and 1.28×10^{-2} mg s⁻¹, respectively, while surface Pd concentrations, evaluated by EDS analysis, were equal to 26 and 23.6 atom %. Comparison of these findings with those at pH 10 indicates that pH reduction has a detrimental effect on the palladium deposition process, but improves the quality of the composite membrane because it appears less damaged (weight loss was about 0.9%) and with narrower pores.

To improve both the quality of the deposit and the efficiency of deposition, the time of deposition was increased from 3 to 9 min, but the improvement was poor. The total amount of Pd deposited increased to 0.221 mg cm⁻², while the deposition efficiency and rate decreased to 19% and 9.8×10^{-3} mg s⁻¹, respectively. The weight loss increased up to about 13% while pores were still partially open. The membrane section-view, reported in Fig. 5, shows spherical particles deposited on the surface tending to form pillars perpendicular to the surface, so that shutting of the pore mouth was partially hindered. Figure 5 shows also the presence of Pd nanoparticles deposited on the lateral surface of pore channels. The distribution of Pd nanoparticles along the channels length was detected by EDS analysis. Figure 6 shows that Pd particles were deposited essentially within a thickness interval from 5 to 10 μm from pores mouth, and not in the central channel part. Figure 6 shows also that the Pd/Al atomic ratio was different in the proximity of the two surfaces, confirming the asymmetry of the membranes.

To increase the amount of Pd deposited and to decrease dissolution, multiple deposition steps (up to five), each lasting 3 min, were conducted. For each deposition step, a fresh solution was used. The amount of Pd deposited increased from 0.104 mg cm⁻², after the

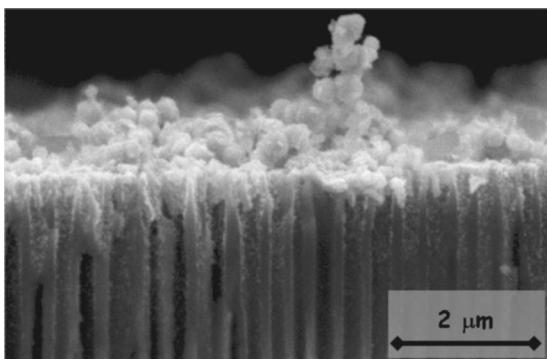


Figure 5. Section view of a Pd-Al₂O₃ composite membranes obtained after 9 min in a deposition bath buffered at pH 8.5 in the presence of NaHCO₃.

first deposition step, to 0.383 mg cm⁻², after 5 deposition steps, while the efficiency of deposition decreased from about 27% down to about 20% after the fifth deposition step, as shown in Fig. 7. This behavior can be explained taking into account that, as the number of the deposition steps increases, surface concentration of free catalytic sites decreases, because they are covered by deposited Pd. Consequently, deposition rate decreases from 1.38 to 1.02 × 10⁻² mg s⁻¹. SEM analysis revealed that after 5 steps pores were still open on both surfaces, which were quite damaged. Note that damage was higher than after one deposition step, indicating that the total immersion time in the plating bath plays a fundamental role in altering the surface morphology of the AAM.

To reduce damage and to restore the concentration of catalytic sites, successive deposition steps (up to four) were alternated with reactivation of the surface. Fresh activation and plating solutions were employed for each step. After four deposition steps a conversion efficiency of about 31% was achieved, but the deposit did not uniformly cover the surface and some pores were still open.

Na₂B₄O₇·H₂O buffer, pH 8.5.— Because the previous deposition procedures did not lead to a dense palladium layer occluding pores, bath composition was modified by substituting NaHCO₃ with a borax buffer, keeping pH at the same value of 8.5. The deposition was performed in 3, 4, or 5 steps, each 3 min long. Analogous to the bath buffered with NaHCO₃, even after 5 deposition steps surface coverage by the metal was not complete. As shown in Fig. 8a, several pores were still open, even if surface coverage is better than in solutions containing NaHCO₃. Following the previous procedure, the successive deposition steps were alternated with reactivation of the surface to restore the concentration of catalytic sites. Figure 8b shows that after the fourth deposition step channels were occluded.

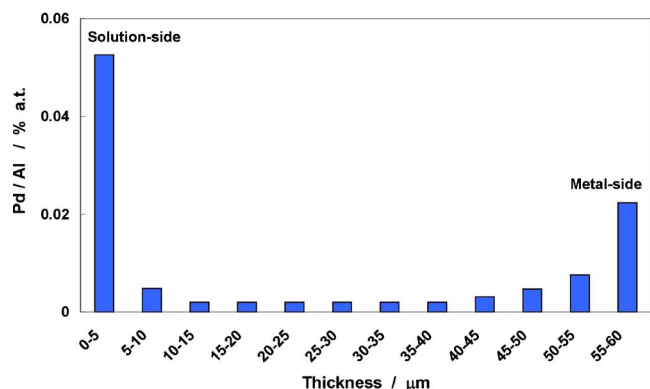


Figure 6. (Color online) EDS analysis along the channel of a Pd-Al₂O₃ composite membranes obtained after 9 min in a deposition bath buffered at pH 8.5 in the presence of NaHCO₃.

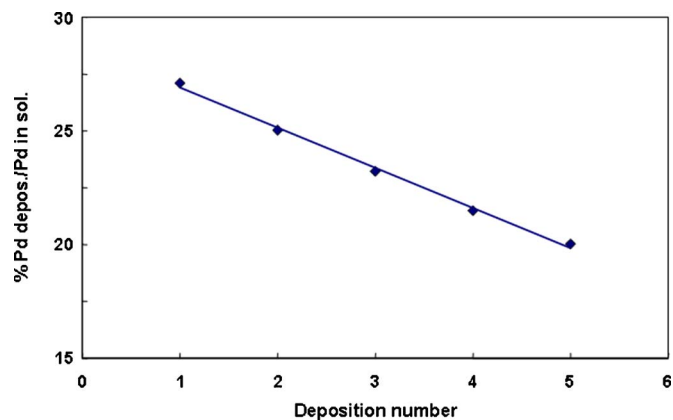


Figure 7. Conversion of Pd vs deposition number in a deposition bath buffered at pH 8.5 in the presence of NaHCO₃.

This conclusion is confirmed by the section view of Fig. 9 showing a dense and continuous palladium film, about 1 μm thick, with good adhesion to the substrate. The amount of Pd deposited was about 0.458 mg cm⁻². This finding indicates a specific influence of the buffer agent on the features of the deposit.

To verify the effectiveness of the procedure adopted, permeability measurements were carried out. Figure 10 shows the fluxes of different gases vs the transmembrane pressure for a composite membrane after three deposition steps. The linear dependence indicates a Knudsen mechanism of gas permeation, described by^{45,46}

$$P_k = \frac{2}{3} \frac{\epsilon r v}{\tau L R T} \quad [5]$$

In Eq. 5, P_k is the permeability coefficient (in mol s⁻¹m⁻²Pa⁻¹),

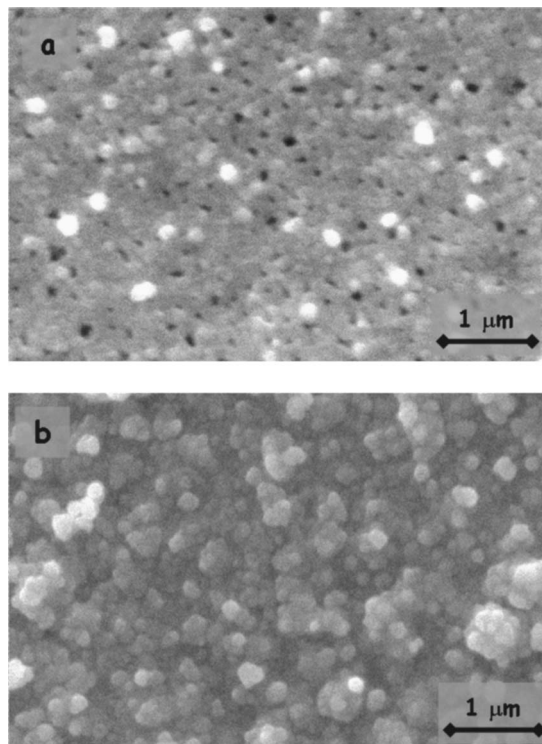


Figure 8. SEM pictures of Pd-Al₂O₃ composite membrane after multiple depositions, each 3 min long, in bath buffered at pH 8.5 in the presence of Na₂B₄O₇·H₂O: (a) after 5 consecutive depositions; and (b) after 4 depositions with intermediate reactivation.

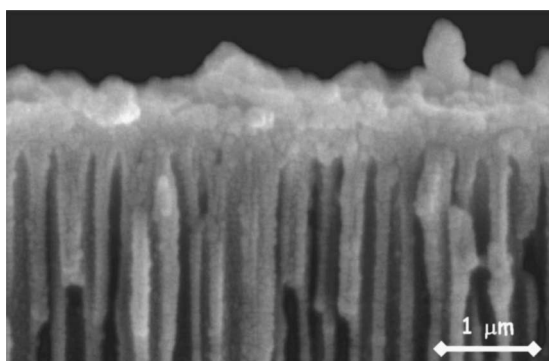


Figure 9. Section view of a Pd-Al₂O₃ composite membrane obtained after 4 deposition steps, each lasting 3 min, with intermediate reactivation, in the bath buffered at pH 8.5 using Na₂B₄O₇·H₂O.

ε the porosity, r the mean pore radius of the membrane, τ the tortuosity factor, equal to unity for uniform straight pores normal to the membrane surface, L the thickness of the membrane, and v the average velocity for an ideal gas given by

$$v = \left(\frac{8RT}{\pi M} \right)^{0.5} \quad [6]$$

where M is the gas molecular weight.

Assuming a Knudsen flow in cylindrical channels, from Eq. 5 and 6, the pore radius can be estimated by the slope of the gas permeability vs $(1/M)^{0.5}$, once known pore population and membrane thickness. This is displayed in Fig. 11 for a membrane obtained after three deposition steps: for this membrane a porosity of 19.6% and a thickness of 57.3 μm were evaluated by SEM analysis, giving a mean pore radius of 54.7 nm. Figure 12 shows the variation of the average pore radius with the number of deposition steps: a relevant decrease occurs after four deposition steps, while the variation between the fourth and the fifth deposition step is negligible. After five deposition steps, the mean pore size of the composite membrane was about 19 nm.

Permeability measurements were also performed on membranes functionalized with deposition steps alternated with reactivation steps, and they confirmed the shutting of the channels shown in Fig. 8b. In fact, nitrogen and methane fluxes were negligible at all transmembrane pressures, while small H₂ and He fluxes were measured through the composite membrane, and they increase sensibly at high transmembrane pressures. Figure 13 shows the gas fluxes of H₂ and He for a membrane functionalized with four deposition steps alternated with surface reactivation: He flux is much lower than that of

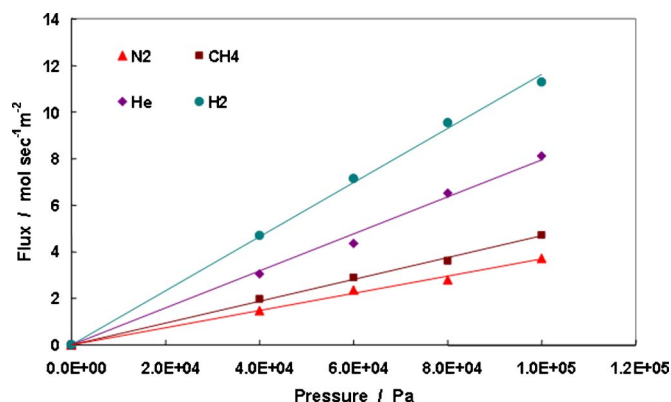


Figure 10. (Color online) Gas flux vs pressure for Pd-Al₂O₃ composite membrane after 3 electroless deposition steps of Pd, each 3 min long, in the bath buffered at pH 8.5 with Na₂B₄O₇·H₂O, $T = 25^\circ\text{C}$.

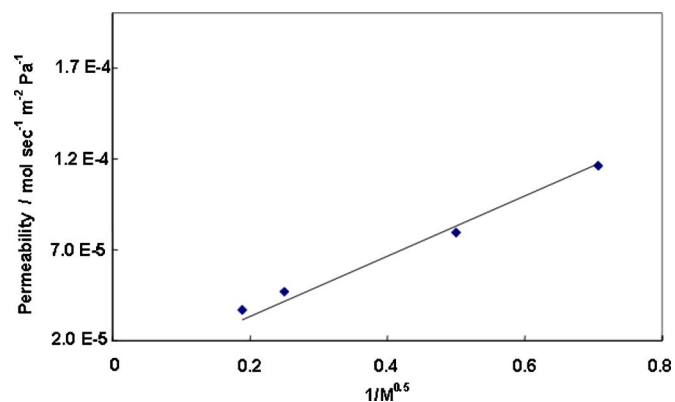


Figure 11. Permeability as function of the inverse square root of molecular weight for the composite membrane of Fig. 10.

H₂. Although metal film appears continuous, He permeation suggests the existence of microholes caused by small impurities and/or surface defects; consequently, H₂ flux should consist of two parts, one coming from the microholes in the palladium layer and the other from the dense part.^{47,48}

The separation factor, defined as the ratio between H₂ and He flux, was calculated at the transmembrane pressure of 0.1 MPa: for composite membranes obtained with reactivation steps this separation factor exceeds the theoretical Knudsen diffusion value, and increases from 2.74 to 6.55 with increasing the number of deposition steps. This improvement of the H₂ separation performance through the Pd-Al₂O₃ composite membranes must be ascribed to the selective surface diffusion transport mechanism.⁴⁵

The higher effectiveness of the bath plating containing Na₂B₄O₇·H₂O in determining pore closure, compared to the identical bath containing NaHCO₃ buffer, was specifically investigated, as it was not reported previously. AAS measurements, carried out on activated membranes held for 3 min in both solutions, revealed a loss of catalytic seeds of about 16% in the presence of NaHCO₃ and 9% in the presence of Na₂B₄O₇·H₂O. This finding indicates that AAMs are slightly more soluble in the plating bath containing the NaHCO₃ buffer, with the consequence that also the catalytic seeds formed in the activation step are partially lost during the electroless deposition. For this reason, the amount of Pd deposited after four steps with reactivation was lower in the presence of NaHCO₃ (0.365 mg cm⁻²) than in the presence of Na₂B₄O₇·H₂O (0.462 mg cm⁻²).

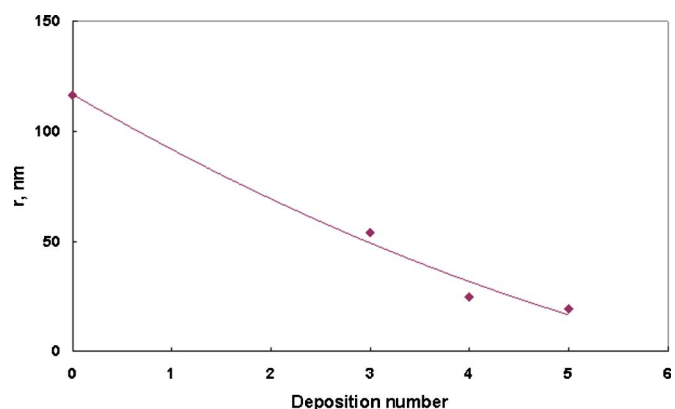


Figure 12. (Color online) Variation of pore radius with the deposition number for Pd-Al₂O₃ composite membranes obtained after multiple depositions, each 3 min long, in bath buffered at pH 8.5 in the presence of Na₂B₄O₇·H₂O.

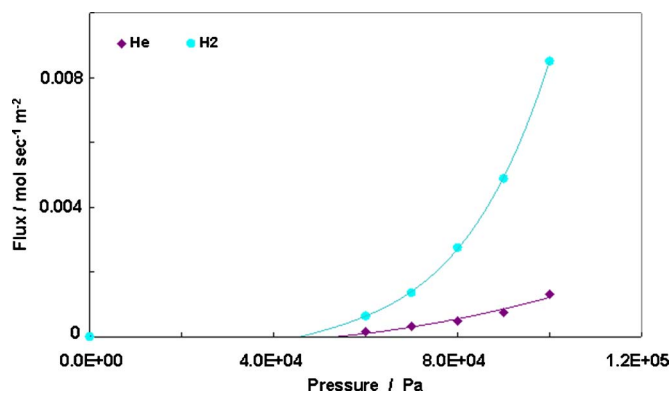


Figure 13. (Color online) Gas flux vs pressure Pd-Al₂O₃ composite membrane after 4 depositions, each 3 min long, with intermediate reactivation in bath buffered at pH 8.5 in the presence of Na₂B₄O₇-H₂O, T = 25 °C.

Conclusions

Electroless deposition of Pd onto AAM is limited by the amorphous nature of the support causing a significant dissolution in the pH interval 9 ÷ 11, where the rate of deposition is maximum. Experiments at pH 10 showed that after 3 min of immersion in the plating bath an efficiency of Pd deposition of about 53% was achieved, but pores were open and the surface of the membrane was heavily damaged. As a result, different procedures were investigated to form a dense metal layer and to find the best compromise between bath utilization and membrane stability. The pH value was lowered to 8.5 and it was controlled by two different buffers: NaHCO₃ or Na₂B₄O₇-H₂O. Despite the lower pH, dissolution of alumina occurred at some extent, as evidenced by the presence on the surface of white alumina/Pd clusters precipitated from the solution. This behavior can be attributable to a local increase of pH due to Pd²⁺ reduction coupled with a local decrease of pH due to hydrazine oxidation. Because the cathodic and anodic areas are in close proximity, alumina dissolved from the cathodic areas precipitated on the anodic ones. The local change of pH did not interfere with the pH of the bulk solution which remained constant during the electroless deposition of Pd.

Single and multiple depositions were carried out to form a dense layer of Pd, and the best results were obtained by using the Na₂B₄O₇-H₂O buffer. Multiple deposition steps were performed using a fresh plating bath after each step, and they were alternated with reactivation steps to restore the surface concentration of catalytic sites.

Permeability measurements showed the progressive closure of the pores with the number of deposition steps. After four deposition steps alternated with surface reactivation, a complete shutting of pores was achieved, owing to the formation of a dense Pd layer permeable only to H₂ and He. The higher effectiveness of the plating bath containing Na₂B₄O₇-H₂O could be due to a lower solubility of amorphous alumina in this solution. Further work is in progress to clarify the transport mechanism of gases and to optimize the plating process for a possible extensive use of these composite membranes for gas separation processes.

Acknowledgments

This work was supported financially by APQ Ricerca della Regione Siciliana Delibera CIPE no. 17/2003, "Laboratorio dell'Innovazione nel Settore dei Beni Culturali."

The Università di Palermo assisted in meeting the publication costs of this article.

References

- S. Ono, M. Saito, M. Ishiguro, and H. Asoh, *J. Electrochem. Soc.*, **151**, B473 (2004).
- S. Ono, M. Saito, and H. Asoh, *Electrochem. Solid-State Lett.*, **7**, B21 (2004).
- S. Ono, M. Saito, and H. Asoh, *Electrochim. Acta*, **51**, 827 (2005).
- Y. Yang and Q. Gao, *Phys. Lett. A*, **333**, 328 (2004).
- J. W. Diggle, T. C. Downie, and C. W. Goulding, *Chem. Rev. (Washington, D.C.)*, **69**, 370 (1969).
- J. P. O'Sullivan and G. C. Wood, *Proc. R. Soc. London, Ser. A*, **317**, 511 (1970).
- J. Siejka, and C. J. Ortega, *J. Electrochem. Soc.*, **124**, 883 (1977).
- K. Shimizu, K. Kobayashi, G. E. Thompson, and G. C. Wood, *Philos. Mag. A*, **66**, 643 (1992).
- V. F. Henley, *Anodic Oxidation of Aluminium and Its Alloys* p. 6, Pergamon Press, Oxford (1982).
- K. Nielsch, F. Muller, A.-P. Li, and U. Gosele, *Adv. Mater. (Weinheim, Ger.)*, **12**, 582 (2000).
- W. G. Yelton, K. B. Pfeifer, and A. W. Staton, *J. Electrochem. Soc.*, **149**, H1 (2002).
- H. Chirac, A. E. Moga, M. Urse, and T.-A. Ovari, *Sens. Actuators, A*, **106**, 348 (2003).
- S. W. Lin, S. C. Chang, R. S. Liu, S. F. Hu, and N. T. Jan, *J. Magn. Magn. Mater.*, **282**, 28 (2004).
- P. Ciambelli, D. Sannino, M. Sarno, and J. B. Nagy, *Adv. Eng. Mater.*, **6**, 804 (2004).
- T. Wu, I. C. Leu, J. H. Yen, and M. H. Hon, *J. Phys. Chem. B*, **109**, 9575 (2005).
- I. Z. Rahman, A. Boboc, K. M. Razeeb, and M. A. Rahman, *J. Magn. Magn. Mater.*, **290-291**, 246 (2005).
- Y. Piao, H. Lim, J. Y. Chang, W.-Y. Lee, and H. Kim, *Electrochim. Acta*, **50**, 2997 (2005).
- X. Zhang, Y. Hao, G. Meng, and L. Zhang, *J. Electrochem. Soc.*, **152**, C664 (2005).
- J. Lee, Y. Yun, J. Oh, and Y. Tak, *Electrochim. Acta*, **51**, 1 (2005).
- R. C. Furneaux, W. R. Rigby, and A. P. Davidson, *Nature (London)*, **337**, 147 (1989).
- P. P. Mardilovich, A. N. Govyadinov, N. I. Mukhurov, A. M. Rzhetskii, and R. Paterson, *J. Membr. Sci.*, **98**, 131 (1995).
- P. P. Mardilovich, A. N. Govyadinov, N. I. Mazurenko, and R. Paterson, *J. Membr. Sci.*, **98**, 143 (1995).
- P. P. Mardilovich, A. N. Govyadinov, N. I. Mukhurov, A. M. Rzhetskii, and R. Paterson, *J. Membr. Sci.*, **98**, 131 (1995).
- J. Randon, P. P. Mardilovich, A. N. Govyadinov, and R. Paterson, *J. Colloid Interface Sci.*, **169**, 335 (1995).
- P. Bocchetta, C. Sunseri, A. Bottino, G. Capannelli, G. Chiavarotti, S. Piazza, and F. Di Quarto, *J. Appl. Electrochem.*, **32**, 977 (2002).
- P. Bocchetta, C. Sunseri, G. Chiavarotti, and F. Di Quarto, *Electrochim. Acta*, **48**, 3175 (2003).
- P. Bocchetta, C. Sunseri, R. Masi, S. Piazza, and F. Di Quarto, *Mater. Sci. Eng., C*, **23**, 1021 (2003).
- R. Dittmeyer, V. Hollein, and K. Daub, *J. Mol. Catal. A: Chem.*, **173**, 135 (2001).
- E. Drioli and M. Romano, *Ind. Eng. Chem. Res.*, **40**, 1277 (2001).
- T. P. Tiemersma, C. S. Patil, M. van Sint Annaland, and J. A. M. Kuipers, *Chem. Eng. Sci.*, **61**, 1602 (2006).
- S. Wieland, T. Melin, and A. Lamm, *Chem. Eng. Sci.*, **57**, 1571 (2002).
- J. Tong, H. Suda, K. Haraya, and Y. Matsumura, *J. Membr. Sci.*, **260**, 10 (2005).
- G. Xomeritakis and Y.-S. Lin, *AIChE J.*, **44**, 174 (1998).
- S.-E. Nam, S.-H. Lee, and K.-H. Lee, *J. Membr. Sci.*, **153**, 163 (1999).
- N. Itoh, N. Tomura, T. Tsuji, M. Hongo, *Microporous Mesoporous Mater.*, **39**, 103 (2000).
- J. N. Keuler, L. Lorenzen, R. N. Sanderson, and V. Linkov, *Plat. Surf. Finish.*, **84**, 34 (1997).
- M. Volpe, R. Inguanta, S. Piazza, and C. Sunseri, *Surf. Coat. Technol.*, **200**, 5800 (2006).
- N. Feldstain, *J. Electrochem. Soc.*, **121**, 738 (1974).
- A. M. T. Van Der Putten, J. De Bakker, and L. G. J. Fakkink, *J. Electrochem. Soc.*, **139**, 3475 (1992).
- J. Horkans, *J. Electrochem. Soc.*, **130**, 311 (1983).
- Y. S. Cheng and K. L. Yeung, *J. Membr. Sci.*, **182**, 195 (2001).
- J. C. Serrano-Ruiz, G. W. Huber, M. A. Sanchez-Castillo, J. A. Dumesic, F. Rodriguez-Reinoso, A. Sepulveda-Escribano, *J. Catal.*, **241**, 378 (2006).
- G. Charlot, *Les Reactions Chimiques En Solution*, p. 402, Masson et Cie, Paris (1969).
- A. R. West, *Solid State Chemistry and Its Applications*, p. 173 John Wiley & Sons Ltd, Chichester (1985).
- A. J. Burggraaf, in *Fundamentals of Inorganic Membrane Science and Technology*, A. J. Burggraaf and L. Cot, Editors, p. 331, Elsevier Science B. V., Amsterdam (1996).
- H. de L. Lyra and R. Paterson, *J. Membr. Sci.*, **206**, 375 (2002).
- H. B. Zhao, K. Pflanz, J. H. Gu, A. W. Li, N. Stroh, H. Brunner, and G. X. Xiong, *J. Membr. Sci.*, **142**, 147 (1998).
- H. B. Zhao, G. X. Xiong, and G. V. Baron, *Catal. Today*, **56**, 89 (2000).